Наносистеми, наноматеріали, нанотехнології
Nanosistemi, Nanomateriali, Nanotehnologii
2021, т. 19, № 4, сс. 923–940

© 2021 ІМФ (Інститут металофізики
ім. Г. В. Курдюмова НАН України)
Надруковано в Україні.

PACS numbers: 61.05.cp, 68.37.Hk, 68.37.Lp, 78.30.Hv, 78.55.Hx, 81.07.Wx, 82.80.Pv

The Effect of Ag Content on the Structural, Optical, and Cytotoxicity Properties of TiO_2 Nanopowders Grown from $TiO(OH)_2$ Precursor by the Chemical Deposition Method

M. Zahornyi[1], N. Tyschenko[1], O. Shyrokov[1], A. Ragulya[1], O. Kolomys[2], V. Strelchuk[2], K. Naumenko[3], L. Biliavska[3], S. Zahorodnia[3], M. Kharchuk[3], M. Skoryk[4], A. Kasumov[1], and A. Ievtushenko[1]

[1]*I. M. Frantsevich Institute for Problems of Materials Science, N.A.S. of Ukraine, 3, Krzhizhanovsky Str., UA-03142 Kyiv, Ukraine*
[2]*V. Ye. Lashkaryov Institute of Semiconductor Physics, N.A.S. of Ukraine, 45, Nauky Prosp., UA-03028 Kyiv, Ukraine*
[3]*D. K. Zabolotny Institute of Microbiology and Virology, N.A.S. of Ukraine, 154, Acad. Zabolotny Str., UA-03143 Kyiv, Ukraine*
[4]*'NanoMedTech' LLC, 68, Antonovych Str., UA-03680 Kyiv, Ukraine*

A series of Ag/TiO_2 is prepared by the chemical deposition method using silver nitrate and suspension of $TiO(OH)_2$ following sonication and treatment up 600°C. Silver nanoparticles are deposited on the surface and inside of TiO_2 nanoparticles depending on the Ag concentration. The Ag/TiO_2 composites are characterized by x-ray diffraction, transmission electron microscopy, scanning electron microscopy, Raman and photoluminescence spectroscopies. The optical activity of Ag/TiO_2 with significant attenuation of photoluminescence in the range of 480–600 nm, a shift of mode E_g from 143 to 150 cm^{-1} and FWHM from 12 to 19 cm^{-1} are revealed due to decreasing of TiO_2 crystallites. The optical activity is increased after loading with Ag because metal particles offer electron traps to decrease the recombination of holes and electrons, especially, with Ag loading of 8 wt.%. The obtained results indicate lower toxicity of nanoparticles in the glycerine + water suspension; regardless of the introduction of silver molecules in amount of 4 or 8 wt.%, their CC_{50} values are of 50 μg/mL and 3.9–58.5 μg/mL for the MDBK and MDCK cells, respectively. Instead, TiO_2 nanoparticles in C_2H_5OH + 1.3-propanediol with the introduction of silver mole-

cules are significantly more toxic for the MDBK cells compared to the pure TiO_2; their CC_{50} values are of 6.5 and 4 μg/mL.

Серію Ag/TiO_2 одержано методом хемічного осадження з використанням нітрату срібла та суспензії $TiO(OH)_2$ після ультразвукового та термооброблення до 600°C. Наночастинки срібла осідають як на поверхні, так усередині наночастинок самого TiO_2 в залежності від концентрації Ag. Композити Ag/TiO_2 було охарактеризовано дифракцією Рентґенівських променів, просвітлювальною електронною мікроскопією, скануванльною електронною мікроскопією, Рамановою та фотолюмінесцентною спектроскопіями. Показано оптичну активність Ag/TiO_2 із значним ослабленням фотолюмінесценції в діяпазоні 480–600 нм, зсувом моди E_g від 143 до 150 $см^{-1}$ і FWHM від 12 до 19 $см^{-1}$ внаслідок зменшення кристалітів TiO_2. Оптична активність зростає зі збільшенням концентрації Ag до 8 мас.%. Одержані результати свідчать про меншу токсичність наночастинок у суспензії гліцерин + вода; незалежно від введення молекул Арґентуму в кількості 4 або 8 мас.%, їх значення CC_{50} становили 50 мкг/мл і 3,9–58,5 мкг/мл для клітин MDBK (нирки бика) та MDCK (нирки собаки) відповідно. Натомість наночастинки TiO_2, розчинені в C_2H_5OH + 1,3-пропандіолі при введенні молекул Арґентуму, були значно більш токсичними для клітин MDBK у порівнянні з чистим TiO_2; їхні значення CC_{50} становили 6,5 та 4 мкг/мл.

Key words: Ag/TiO_2, irradiation, Raman spectra, photoluminescence, defects, optical activity, cytotoxicity.

Ключові слова: Ag/TiO_2, опромінення, Раманові спектри, фотолюмінесценція, дефекти, оптична активність, цитотоксичність.

(Received 2 February, 2021)

1. INTRODUCTION

Titanium dioxide was used as a photocatalyst and has attracted scientific interest for many years [1–3]. Heterogeneous photocatalytic oxidation is a promising technique for the complete oxidation of dilute organic pollutants in the waste gas stream. Many organics, bacteria, virus can be oxidized to CO_2 and H_2O at room temperature with TiO_2 catalysts in the air when illuminated with UV or near-UV light. The UV light excites electrons from the valence band to the conduction band. The resulting electron/hole pairs can then migrate to the surface and initiate redox reactions with adsorbed organics.

Nowadays, different kinds of methods, including shape, size, and facet control, element doping have been developed to effectively enhance the photocatalytic performance through increasing the broad absorption of sunlight, prolonging the lifetime of photoinduced carriers, and enhancing the optical activity and photocatalytic stability of TiO_2. For example, *via* shape control, doping with metal or non-

metal elements, dye-sensitization, and construction of heterostructured photocatalyst systems by combining them with plasmonic metals (*i.e.*, Ag, Au, Pd, Pt) or other semiconductors [4–10]. Noble metal nanoparticles (NPs) can show SPR (surface plasmonic resonance), which can be tailored by engineering the shape, size, and surroundings [7–10]. Therefore, noble metal NPs cannot only strongly absorb visible light but also can serve as an electron sink and source of active reaction sites [11].

Morphology-controlled rutile titanium (IV) oxide (TiO_2) and anatase TiO_2 usually prepared by a hydrothermal method and their surfaces were selectively loaded with Au, Ag, and Au–Ag bimetallic nanoparticles (NPs) by photo-deposition to obtain visible light-responsive photocatalysts [12].

The authors [13–14] note that when doped with metals (rare earth) elements, it is possible to shift to the visible region, but the photocatalytic activity decreases, especially in the UV range. For the electronic interaction, nitrogen is good because electrons can pass for the dopant of the orbitals 2*p* or 3*p* to the 3*d* orbital Ti, and the width of the forbidden band decreases.

TiO_2 powders doped with Ag, Fe enhanced the photocatalytic and bactericidal activity [15–18]. For example, Ag concentration from 2.46 to 6.0 wt.% showed increasing of bacteriophage virus inactivation rate 7 times. Therefore, the duration of the disinfection process reduced from 5 to 0.75 min [15]. Der-Shing Lee, Yu-Won Chen have shown the optimum Ag loading (2 wt.%) for excellent methylene blue destruction under UV-light irradiation [18].

The bactericidal effect on bacillus Kochi has been studied using TiO_2–Ag–SiO_2 photocatalyst [17]. The synthesized composite characterized by a higher surface area 164 $m^2 \cdot g^{-1}$ in comparison with P25. Thus, the ability to inactivate composite photocatalyst occurs over a wide spectral range of UV irradiation with an intensity of 2.5 $mV \cdot cm^{-2}$. However, the high absorbance of visible light does not always increase the photocatalytic activity. Sometimes, cation doping leads to a certain number of defects in TiO_2, which can act as centres for the recombination of charges.

Ag–TiO_2 were coated on glass substrates with different dopant concentrations (1%, 3%, 5%, 7% and 10%) and annealed at 550°C [19]. The crystalline structure and phase formation of Ag–TiO_2 was examined using XRD. The HRTEM analysis of pure and 5% Ag-doped TiO_2 thin films was revealed that the particles are spherical with sizes around 23.8 and 11.6 nm, respectively. The Raman spectrometer was also used to identify the phase formation and vibrational modes in the prepared silver-doped TiO_2 coatings. Ag-doped TiO_2 nanoparticles show characteristic photoluminescence (PL) corresponding to the visible spectral range with excitation at 325 nm.

The intensity of luminescence emission decreases with doping of silver ions due to decreasing bandgap TiO_2 from 3.2 to 2.7 eV.

Considering the methods of synthesis and study of nanocomposite properties with oxide NPs, especially of TiO_2–Ag (Au), has not yet received information on the effectiveness of their use. The reason for all would be to use expensive isopropoxide (butoxide), precursors. Using cheap $TiCl_4$ as the precursor of TiO_2 does not allow obtaining the composite system with the required properties due to the complexity of the control of the hydrolysis process, the difficulties associated with the removal and the highly reactive reaction by-products (HCl). However, methods of surface modification of TiO_2 in the synthesis of composites in most cases do not cause difficulties and apply industrial processes.

Therefore, the modification of TiO_2 with Ag has attracted interest for optical and photocatalytic applications. The silver ion-doped TiO_2 attracts much attention due to its outstanding photocatalytic activity and antibacterial activity. However, the withdrawal of nanosize powder catalyst particles from the liquid suspension is difficult. This leads to the formation of secondary pollution and can be catalyst loss activity.

The present paper focuses on the surface structure, cytotoxicity, spectroscopic features (light irradiation 325, 488 nm) of Ag/TiO_2 series prepared by chemical deposition method using silver nitrate, and suspension of $TiO(OH)_2$. The effect of Ag-loading at 4 wt.% and 8 wt.% on the microstructure, Raman and photoluminescence properties are studied and discussed.

2. EXPERIMENTAL

2.1. Synthesis of TiO_2/Ag

The raw material for obtaining the sample was a suspension of hydrated titanium dioxide $TiO(OH)_2$ (metatitanic acid), which is a product of the intermediate stage of processing of titanium concentrates and slags at the plant ‘Sumykhimprom’. The suspension was heated at 600°C with a heating rate of 5°C/min to obtain TiO_2 powder. Nanosize particles of titanium dioxide modified with silver were obtained in aqueous solutions of $TiO(OH)_2$ by adding alkali to form anatase modification with a range of silver concentrations from 0 to 8 wt.%. Samples number TiO_2, ATO4 (4 wt.% Ag), ATO8 (8 wt.% Ag).

2.2. Characterization

The crystalline nature and phase formation of Ag–TiO_2 powders are

known using powder x-ray diffractometer (DRON 3M) with cobalt anode tube. Mira 3 Tescan with EDX (Oxford INCA *x*-act) was used to study morphology and elemental analysis. The particle shape and size are found with high-resolution transmission electron microscopy (TEM JEM-1400). TEM study of the morphological features of nanoparticles was conducted. The obtained suspensions were mixed actively for 5 min. The drops of the finished suspensions were placed on copper grids coated with a formvar film, which was reinforced with carbon. The samples of nanoparticles dried at room temperature were analysed using a TEM JEM-1400 (Jeol, Japan) at an accelerating voltage of 80 kV. Electron diffraction of nanoparticles was performed on TEM with the same accelerating voltage, with the introduction of a field aperture and removal of an objective aperture. Raman spectroscopy, photoluminescence emission spectra of powders (Horiba Jobin-Yvon T64000) was used to study the structural properties of silver ions doped TiO_2 powders using Ar–Cr laser at 488 nm for Raman and He–Cd laser at 325 nm for PL.

2.3. CYTOTOXICITY ASSAY

MTT-assay was used for the analysis of cell viability [19]. The MDCK cells (Madin–Darby canine kidney cells) obtained from the Institute of Epidemiology and Infectious Diseases Named after L. V. Gromashevsky of the Academy of Medical Sciences of Ukraine and the MDBK cells (Madin–Darby bovine kidney cells) obtained from the tissue culture collection of the Institute of Virology of the Bulgarian Academy of Sciences were used.

Cells were maintained in sterile plastic falcon (Sarstedt, Germany) in a growth medium composed of 45% DMEM (Sigma, USA), 45% RPMI 1640 (Sigma, USA) and 10% foetal bovine serum (Sigma, USA) heat inactivated at 56°C, with antibiotic gentamycin (100 μg/mL) (Sigma, USA).

For the study, the attached cells were trypsinizated for 3–5 min, and then cells were counted and distributed in 96-well plate with density 30.000–50.000 cells in each well. The plate was incubated for 24 h at 37°C in a 5% CO_2 atmosphere to allow the cells to attach to the bottom of the well. After 24 h of growing, monolayer of the MDBK and MDCK cells in 96-multiwell plates were incubated with TiO_2 nanoparticles (NPs) at concentrations of 100, 10.0, 1.0, and 0.1 μg/mL. Nanoparticles were diluted in growth medium for cell cultures. Control cells were incubated with fresh medium lacking NPs for 72 h. A total of 20 μL of MTT solution 3-(4.5-dimethylthiazol-2-yl)-2.5-diphenyl tetrazolium bromide (Sigma-Aldrich, USA) was added to wells and cells were incubated at 37 °C and 5% CO_2 for 3–4 h, then the medium was removed and 150 μL

of 96% ethanol was added. The plates were read using a Multiskan FC (Thermo Scientific, USA) with a 538-nm test wavelength. The percentage of cell viability under the condition of TiO_2 NPs action was calculated using formula:

$$\% \text{ of cell viability (or mitochondrial activity)} = A/B \cdot 100,$$

where A is the mean optical density of the studied samples at a certain concentration, and B is the mean optical density of the control cell samples. NPs concentration, at which cell viability was inhibited by 50% (CC_{50}), was estimated in comparison to the control cells not treated with NPs.

3. RESULTS AND DISCUSSION

3.1. XRD Analysis

X-ray diffraction (XRD) patterns used to examine the phase identification and structural properties of the Ag–TiO_2 powders. Figure 1 shows the XRD pattern of Ag doped TiO_2 powders. The observed XRD patterns of all Ag–TiO_2 series well matched with standard JCPDS File No: 894921. XRD results clearly show that the Ag–TiO_2 powders revealed the formation of a tetragonal anatase. The TiO_2 powders showed several diffraction peaks at $2\theta = 25.34°$, 37.83°, 48.11°, 53.94°, 55.15°, 62.79° were indexed as (101), (004), (200), (105), (211), respectively, which close to values [20]. In our observation, the diffraction pattern of Ag–TiO_2 powders exhibit, no oth-

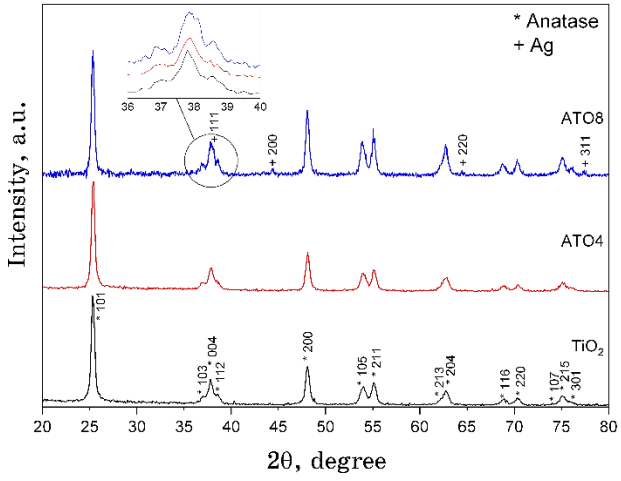

Fig. 1. XRD patterns of TiO_2–Ag

er peaks related to the brookite or rutile phase, which indicates that the powders are in a single anatase phase. In case of lower amount of Ag doped TiO_2 (4 wt.%), no extra peak assigned to Ag was founded, feasibly due to highly dispersion. However, at higher amount of Ag (8 wt.%) doping, the weak diffraction signal is appeared at $2\theta = 38.15°$, 44.38°, 64.45°, and 77.32° corresponding to metallic Ag (JCPDS #89–3722) having a cubic crystalline structure with parameter lattice $a = 4.0862$ close to [21]. When the doping of Ag, a strain is induced in the TiO_2 crystal lattice due to the occurrence of ionic radii mismatch, the ionic radii of Ag^+ (1.26 Å) being greater than Ti^{4+} (0.68 Å) permits only a little amount of Ag^+ going into the periodic crystal lattice of TiO_2 by replacing the Ti^{4+} ions [20] changing of the lattice periodicity. In addition, the parameter FWHM at $2\theta = 25.3°$ is decreased from 0.4101 to 0.3815 (Table 1) may be due to defects contribution on the surface of TiO_2.

3.2. EDX

The EDX method (Fig. 2) found that the content of elements for pure TiO_2: Ti—54.25 wt.%; O—43.93 wt.%, S—0.5 wt.%. The S content can be explained as follows, the raw material $TiO(OH)_2$ synthesized by a specific technology of the plant 'Sumykhimprom' in sulphuric acid. Therefore, even with repeated washing powder, the sulphur residue is in the raw material. The content of elements for doped TiO_2: Ti—46.27 wt.%; O—49.69 wt.%, S—0.14 wt.%, Ag—3.3 wt.%. There is also an amount of carbon. The results obtained by the EDX method indicate the non-stoichiometry of oxide nanopowders ($Ti/O < 2$).

3.3. TEM

The morphology of materials such as shape and particle size is analysed by TEM. Figure 3, *a*–*c* show the morphologies of the Ag/TiO_2 samples. Ag nanoparticles on TiO_2 support were dispersed and the sizes of Ag nanoparticles were 35–40 nm. There was no clear correlation between Ag loading and Ag particle size because Ag particles were very homogeneously distributed. Moreover, the sizes of TiO_2 initial particles were 20–30 nm. After loading of Ag, the sizes of TiO_2 particles decreased to 13–20 nm. A 'ball-shaped' particles of silver with developed crystalline structure in TiO_2 (diffraction electrons) were observed.

The results in Figure 4 show that TiO_2 can be present in tetragonal phase (defected state), and Ag phase with a cubic crystalline structure (sample ATO8), which correlate with XRD results.

TABLE 1. The structural parameters of TiO_2, and Ag/TiO_2 powders.

Sample	2θ	*FWHM*	*d*, Å	Phase
TiO_2	25.32	0.3895	3.5170	*
	36.93	0.5045	2.4339	*
	37.79	0.4968	2.3806	*
	38.58	0.4422	2.3335	*
	48.04	0.4245	1.8940	*
	53.91	0.6804	1.7007	*
	55.06	0.4757	1.6680	*
	62.16	0.5637	1.4934	*
	62.72	0.5476	1.4813	*
	68.82	0.5391	1.3642	*
	70.31	0.6221	1.3390	*
	74.03	0.4632	1.2806	*
	75.07	0.5369	1.2654	*
	76.01	0.7301	1.2520	*
ATO4	25.34	0.3831	3.5151	*
	36.93	0.4868	2.4341	*
	37.84	0.5308	2.3777	*
	38.55	0.4492	2.3355	*
	48.08	0.4309	1.8925	*
	53.95	0.5664	1.6997	*
	55.10	0.4767	1.6667	*
	62.13	0.6087	1.4941	*
	62.68	0.7564	1.4822	*
	68.84	0.6463	1.3638	*
	70.39	0.4573	1.3376	*
	74.04	0.5725	1.2804	*
	75.08	0.6040	1.2652	*
	76.03	0.6777	1.2518	*
ATO8	25.31	3.5185	0.3676	*
	36.92	2.4348	0.4257	*
	37.80	2.3799	0.3955	*
	38.12	2.3609	0.1922	+
	38.57	2.3341	0.2670	*
	44.32	2.0437	0.2485	+
	48.05	1.8937	0.3689	*
	53.88	1.7017	0.4026	*
	55.08	1.6674	0.4144	*
	62.10	1.4947	0.5067	*
	62.71	1.4816	0.4412	*
	64.44	1.4459	0.1512	+
	68.76	1.3653	0.5403	*
	70.29	1.3392	0.4155	*
	74.01	1.2808	0.4600	*
	75.08	1.2652	0.5057	*
	76.04	1.2516	0.3850	*
	77.36	1.2335	0.1786	+

Note: ATO—argentum titanium dioxide, *—anatase, +—Ag.

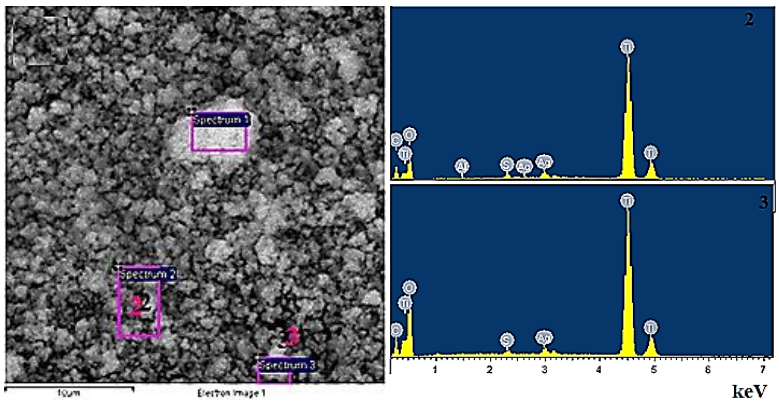

$TiO_2 + 4\%$ Ag

a *b*

Fig. 2. SEM micrograph (*a*) and EDX spectra 2–3 (*b*) of the ATO4 powder.

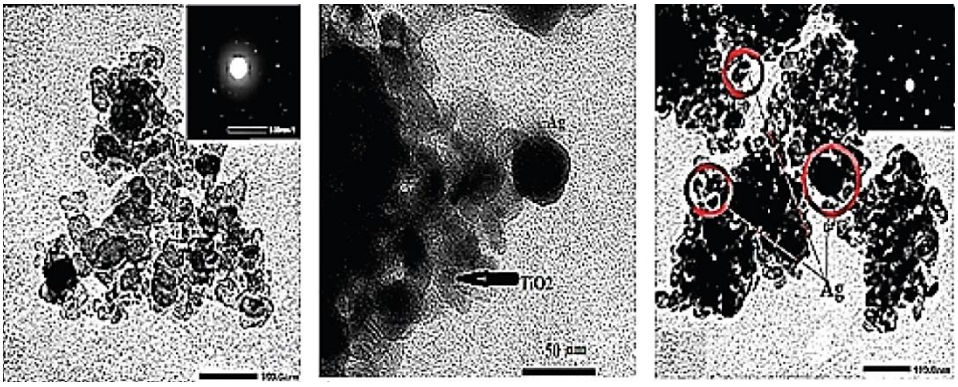

a *b* *c*

Fig. 3. TEM images of pure TiO_2 (*a*), ATO4 (*b*), and ATO8 (*c*) powders.

The hydroxyl group content on the TiO_2 surface samples is important for antimicrobial and photocatalytic properties because in the process of UV irradiation OH groups on the defective surface of TiO_2 are active due to hole capture with subsequent formation of $\cdot$OH radicals for the destructive of toxic organic substances or pathogens. Besides, the presence of silver provides an efficient process of photogeneration of electrons, their transfer from the conduction band Ag to the TiO_2 with the subsequent formation of the Schottky barrier, which inhibits the rate of recombination of photogenerated charges.

Ag and TiO_2 have different work functions, ($\Phi TiO_2 = 4.2$ eV, $\Phi Ag = 4.6$ eV) and hence, when silver is in contact with TiO_2, elec-

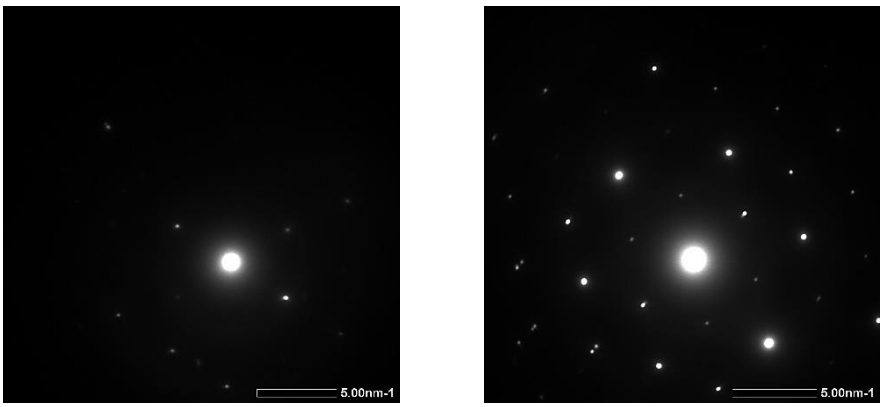

a *b*

Fig. 4. Electron diffraction of pure TiO_2 (*a*), ATO8 (*b*) powder.

trons will transfer from TiO_2 to silver. These electrons transfer to silver, and loads on the surface of silver will be scavenged by the electron acceptor, thus decrease the recombination between electrons and holes; thereby, silver atoms act as electron traps. The electron-hole recombination is the main reason for low efficiency of TiO_2 photocatalysts [20–24]. Therefore, the existence of silver atom in Ag/TiO_2 can facilitate the transport of more holes to the surface and enhance the optical activity. The Ag particles on TiO_2 act as electron-hole separation centres. The photo-generated electrons transferred from the TiO_2 conduction band to metallic silver particles on TiO_2 are thermodynamically possible, because the Fermi level of TiO_2 is higher than that of silver metals [23, 24]. The Schottky barrier is formed at the $Ag–TiO_2$ contact region, which improved the charge separation and thus retards the recombination of the photo-generated electrons and holes. The photogenerated electrons accumulated on the surface of Ag have a good fluidity and can be transferred to oxygen molecules, which is absorbed on the surface of Ag.

3.4. Raman

Figure 5 shows the Raman spectra of Ag doped TiO_2 powders. The powders showed several Raman bands located at 142 cm^{-1} (E_g), 196 cm^{-1} (E_g), 396 cm^{-1} (B_{1g}), 513 cm^{-1} ($A_{1g} + B_{1g}$), and 636 cm^{-1} (E_g), which is close to [25]. The strong and sharp Raman peak located at 142 cm^{-1}, which denotes the formation of the anatase phase [21, 25]. In our observation, the Raman spectra of $Ag–TiO_2$ powders exhibit no other peaks for the brookite/rutile phase, which confirms

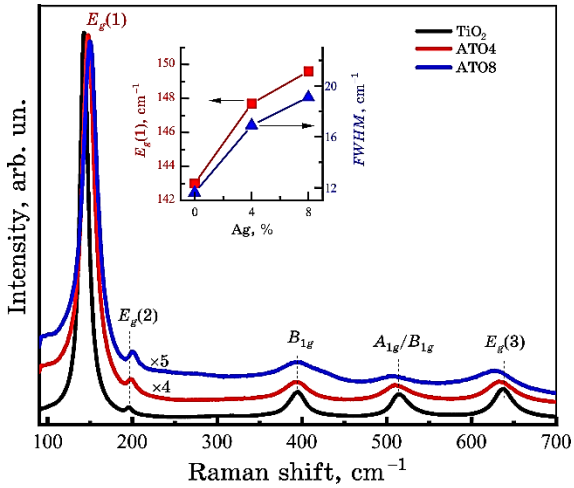

Fig. 5. Raman spectra of TiO_2 (*1*), ATO4 (*2*), ATO8 (*3*) powders.

that all powders are in a single anatase phase (correlation with XRD). The peak intensities found to decrease whereas the width of peak increases because of the lattice distortion and presence of defect levels. The most intense band E_g (1) is shifted in the high-frequency side from 142 to 149 cm^{-1}, while its half-width (FWHM) increases from 11 to 19 cm^{-1}. Lattice deformation, defects and crystallite size have a strong influence on the shear, expansion of peaks and the intensity of Raman peaks [26].

According to the calibration curve [27], we obtained that the average size of anatase crystallites for doped powders is 10 and 8 nm at a silver content of 4 and 8 wt.%, respectively. As well known, the doping with metal ions in the optimal concentration prevents the growth of nanocrystallites [28]. The decrease in the size of TiO_2 particles when replacing Ti^{4+} ions with Ag^{+} ions is associated with the passivation of the boundaries of TiO_2 grains by doping impurity ions, which leads to a violation of structural symmetry, and hence to reduce nanoparticle sizes [29]. TEM images of the samples are confirmed too. The doping by the silver to maintain charge neutrality creates oxygen vacancies in the TiO_2 lattice. If the silver ion replaces the Ti^{4+} ion during doping, the bonds of the Ti–O–Ti complex will be distorted and new bonds of the Ag–O–Ti or Ag–O–Ag complexes will be formed. Therefore, the disruption of Ti–O–Ti bonds and the formation of new Ag–O bonds will affect the combination-active modes and will lead to the expansion and shift of the bands for Raman TiO_2 doped with silver.

There is a high-frequency shift and increase in the half-width of the E_g (1) band at 142 cm^{-1} and E_g (2) band at 196 cm^{-1}, while the

B_{1g} band at 636 cm^{-1} and A_{1g} /B_{1g} at 513 cm^{-1} show a low-frequency shift and a significant increase in half-width in the Raman spectra of silver-doped nanopowders. A wide complex band in the range of 220–300 cm^{-1} is due to the processes of multiphonon scattering [30]. Since in the Raman spectra all oscillations move mainly oxygen atoms, the introduction of silver atoms changes the local coordination of oxygen around Ti^{4+}.

The appearance of structural defects because of doping, which leads to a distortion of octahedra of crystal structure TiO_6, the occurrence of oxygen vacancies, Ti^{4+} ions, surface states, must be accompanied by changes in radiative recombination due to changes in the electronic structure within the bandgap. This primarily refers to the recombination of autolocalized excitons at TiO_6 centres and radiation associated with different *F*-centres due to the presence of oxygen vacancies [31]. The location of the radiation bands, as well as changes in their positions and intensities, depend on the size of TiO_2 nanocrystals and the concentration of the doping impurity, which determine the type and density of donor and acceptor centres on the oxide surface and, as a consequence, photoluminescence spectra [32].

3.5 PL Spectra

Figure 6 shows the photoluminescence analysis of Ag/TiO_2 doped series. The addition of silver atoms leads to a significant (15 times)

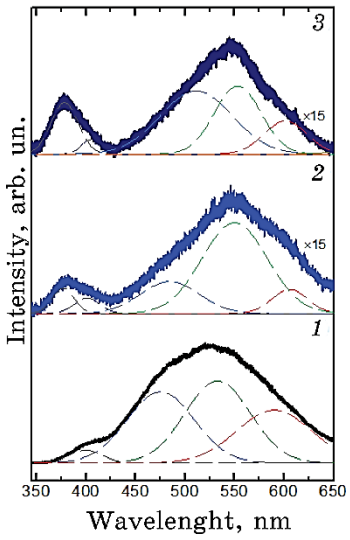

Fig. 6. PL spectra of TiO_2 (*1*), ATO4 (*2*), ATO8 (*3*) powders.

quenching of photoluminescence. For TiO_2 powder with 8 wt.% silver atoms, it has a more pronounced character than with an Ag content of 4 wt.%. This attenuation of the photoluminescence intensity indicates a general decrease in the mutual recombination of photoinduced charge carriers. The doping by silver atoms causes not only general damping of the PL intensity but also a shift and decrease in the band intensity in the region of 480–490 nm, which corresponds to the recombination of autolocalized excitons due to distortion of the TiO_6 octahedron.

The latter is possible both due to the displacement of Ti and O atoms due to substitution by a much larger Ag atom and due to a change in their ionic state, which is manifested in the interatomic bonds in the TiO_6 octahedron. The nature of TiO_6 distortions, in turn, affects the possibility of autolocalization of excitons and, thus, the increase in the probability of photogenerated charges coming to the surface, which can further improve the photocatalytic reactions involving TiO_2. In addition, there is a redistribution of intensity between the bands due to the recombination of autolocalized excitons and the radiation of *F*-centres. The high-frequency shift of all these lines may be due to changes in the size of the nanocrystallites, which is confirmed by the results of Raman spectroscopy. The oxygen vacancies in the TiO_2 lattice are a kind of intrinsic defect, which creates intermediate energy states within the bandgap of titania. These oxygen vacancies act as photoinduced electron (e^-) and hole (h^+) pair recombination centres. Therefore, this emission has occurred from the recombination of e^-/h^+ pair via oxygen vacancies.

Thus, oxygen vacancies form both in the volume of nanocrystals and on their surface, it is possible to form several localized electronic states for anatase. In addition, it should also be noted that in the process of photochemical transformations the formation of new donor and acceptor levels. Thus, the energy electron structure within the bandgap in nanocrystalline doped Ag/TiO_2 samples can be complex. Therefore, it contributes to the sensitization of semiconductor nanoparticles to visible light, thus, improves the relaxation of electronic excitation, and therefore complicates the understanding of the nature and dynamics of photochemical transformations necessary to create conditions that reduce losses of photogenerated charge carriers.

3.6. Cytotoxicity of Suspensions with Powders TiO_2–AG

Determination of the cytotoxicity of titanium dioxide (TiO_2) with different percentages of argentum (Ag) is an integral component of any drug development process. The research was carried out using

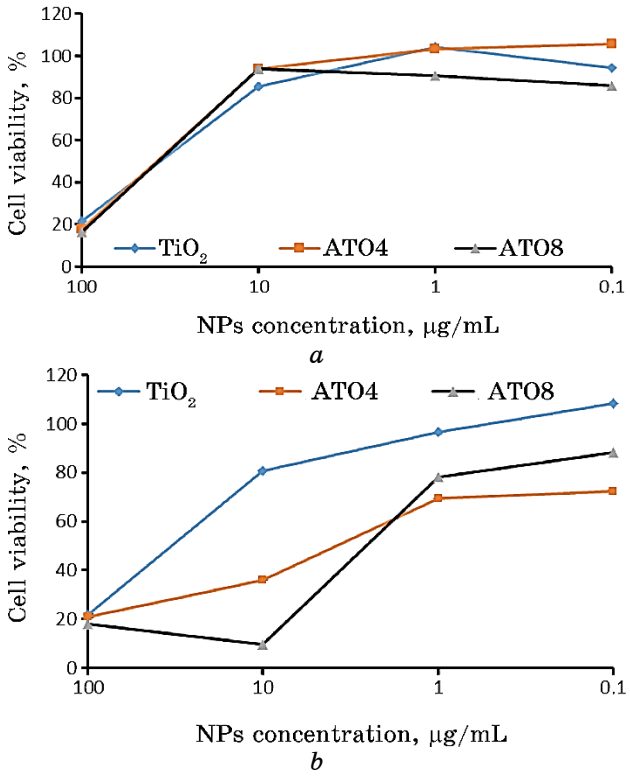

Fig. 7. The effects of the TiO_2 NPs in glycerine + water suspension (*a*) and in a C_2H_5OH + 1,3-propandiol suspension (*b*) on the viability of the MDBK cells.

the MTT-assay.

It was shown that TiO_2 NPs in glycerine + water suspension possess significant cytotoxicity at concentrations of 100 μg/mL, as MDBK cells viability decreased by more than 84% (Fig. 7, *a*). However, at a concentrations of 10.0÷0.1 μg/mL, they were non-toxic because reduced cell viability by a maximum of 15%. TiO_2 NPs with Ag (4–8 wt.%) in C_2H_5OH + 1.3-propanediol suspension at a concentration of 100 and 10 μg/mL were toxic for MDBK cells, as they suppressed their viability by 65–91% (Fig. 7, *b*).

As shown in Figure 8, *a*, the composition of TiO_2 without Ag, with 4 wt.% and 8 wt.% Ag in glycerine + water were less toxic on the MDCK cells compare to nanoparticles of TiO_2 in the C_2H_5OH + 1.3-propandiol. Thus, these samples do not decrease the cell viability at a concentration from 0.1 to 10 μg/ml. The inhibition of mitochondrial activity detects only at a concentration of 100 μg/ml, the percentage of life were at range from 8 to 33%.

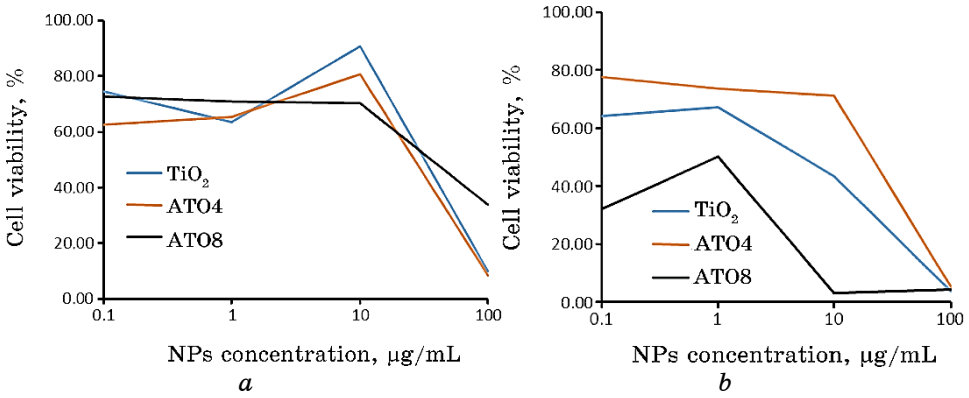

Fig. 8. Viability of the MDCK cells cultivated on the different samples of TiO_2 and TiO_2 with Ag in glycerine + water (*a*) and at C_2H_5OH + 1,3 propandiol (*b*).

Our results on the MDCK cell line clearly show that TiO_2 with 8 wt.% Ag in the C_2H_5OH + 1,3-propandiol was highly toxic at a concentration of 10 and 100 μg/ml. The inhibition of cell viability was 97% (Fig. 8, *b*). Other samples, TiO_2 without Ag and TiO_2 with 4 wt.% Ag were toxic only at a high concentration of 100 μg/ml. Thus, the inhibition of mitochondrial activity was 96%. It should be noted that in minimal dilution inhibition of cell viability decreased to the control sample.

Using the linear regression model in Microsoft Excel (predictor function) [32] and dose-dependent values of the NP cytotoxicity, it was estimated that for MDBK cells the CC_{50} indexes of TiO_2 NPs regardless of the solvent equalled 50 μg/mL (Table 2), while, for MDCK cells, the CC_{50} index of TiO_2 diluted at C_2H_5OH + 1.3-propandiol was lower in 2.5 times as compared with glycerine + water suspension. The obtained results indicate lower toxicity of nanoparticles in the glycerine + water suspension, regardless of

TABLE 2. NPs concentration, at which cell viability was inhibited by 50%.

Solvent—glycerine + water			
Type of cells	TiO_2	ATO4	ATO8
CC_{50} (for the MDBK cells), μg/mL	50	50	50
CC_{50} (for the MDCK cells), μg/mL	42.8	39	58.3
Solvent—C_2H_5OH + 1.3-propandiol			
CC_{50} (for the MDBK cells), μg/mL	50	6.5	4
CC_{50} (for the MDCK cells), μg/mL	17.4	36.9	2.3

the introduction of silver molecules amount of 4 or 8 wt.%, their CC_{50} values were 50 μg/mL and 3.9–58.5 μg/mL for the MDBK and MDCK cells, respectively. Instead, TiO_2 nanoparticles in C_2H_5OH + 1.3-propanediol with the introduction of silver molecules were significantly more toxic for the MDBK cells compared to the pure TiO_2 NP, their CC_{50} values were 6.5 and 4 μg/mL.

4. CONCLUSIONS

Nanopowders Ag/TiO_2 successfully obtained by chemical deposition technique. The effect of Ag concentration on the structural, morphological, cytotoxicity and optical properties, PL emission behaviour has been systematically studied. The crystallite size decreased with cumulative concentrations of Ag doping. The crystalline phase of the $Ag–TiO_2$ was confirmed using XRD, and Raman analysis. The average size of pure and 8 wt.% Ag^+ doped TiO_2 particle was determined to be 25–30 and 13–15 nm, respectively, using the TEM images. The optical activity of Ag/TiO_2 with significant attenuation of photoluminescence in the range of 480–600 nm, a shift of mode E_g from 143 to 150 cm^{-1} and FWHM from 12 to 19 cm^{-1} was stated due to decreasing of TiO_2 crystallites to 8 nm. As a result of the cytotoxicity studies, it was shown that the type of solvent depends on the toxicity level of the studied nanoparticles for the cell cultures. Thus, the studied nanocomposites in C_2H_5OH + 1.3-propanediol increases the inhibition of cell viability compared to nanoparticles in glycerine + water. In addition, it was determined that increasing the concentration of silver leads to increased cytotoxicity for cell cultures. The results obtained made it possible to determine CC_{50} values, which are the primary test for subsequent antiviral activities.

ACKNOWLEDGEMENTS

This work was partially supported by the research project of N.A.S. of Ukraine ‘The development of photocatalytic nanocomposites for viruses inactivation in the air’ (No. 40/20-H) and was partially supported by the research projects of NAS of Ukraine ‘Development of innovative photocatalytic nanostructured materials based on ZnO and TiO_2’ (528/IPM-11/20).

REFERENCES

1. M. N. Ghazzal, H. Kebaili, M. Joseph, D. P. Debecker, P. Eloy, J. De Coninck, and E. M. Gaigneaux, *Appl. Catalys. B: Environm.*, **115**: 276

(2012); doi:10.1016/j.apcatb.2011.12.016
2. A. L. Luna, D. Dragoe, K. Wang, B. Peaunier, E. Kowalska, B. Ohtani, and C. Colbeau-Justin, *The J. Physic. Chem. C*, **121**: 14302 (2017); doi:10.1021/acs.jpcc.7b01167
3. G. V. Sokolsky, M. N. Zahornyi, T. F. Lobunets, N. I. Tyschenko, A. V. Shyrokov, A. V. Ragulya, S. V. Ivanov, N. Gayuk, and V. E. Sokol'skii, *Journal of Chemistry and Technologies*, **27**: 130 (2019); doi:10.15421/081914
4. Yu. B. Pankivskka, L. O. Biliavska, O. Yu. Povnitsa, M. M. Zagornyi, A. V. Ragulia, M. S. Kharchuk, and S. D. Zagorodnya, *Microbiol. J.*, **81**: 73 (2019); doi:10.15407/microbiolj81.05.073
5. J. Li, and N. Wu, *Catalys. Sci. & Technol.*, **5**: 1360 (2015); doi:10.1039/c4cy00974f
6. A. Ievtushenko, N. Karpyna, J. Eriksson, I. Tsiaoussis, I. Shtepliuk, G. Lashkarev, R. Yakimova, and V. Khranovskyy, *Superlattices and Microstructures*, **117**: 121 (2018); doi:10.1016/j.spmi.2018.03.029
7. A. Zaleska-Medynska, *Metal Oxide-Based Photocatalysis. Fundamentals and Prospects for Application* (Book Elsiver: 2018).
8. H. Harada, A. Onoda, T. Uematsu, S. Kuwabata, and T. Hayashi, *Langmuir*, **32**: 6459 (2016); doi:10.1021/acs.langmuir.6b01073
9. O. M. Lavrynenko, M. N. Zahornyi, M. M. Bataiev, Yu. M. Bataiev, O. Yu. Pavlenko, and O. A. Kornienko, *Khimiya, Fizika ta Tekhnologiya Poverkhni*, **11**: 508 (2020); https://doi.org/10.15407/hftp11.04.508
10. P. Nguyen-Tri, V. Nguyen, and T. Nguyen, *Journal of Composites Science*, **3**, No. 2: 34 (2019); doi:10.3390/jcs3020034
11. M. Zahornyi, *Powder Metallurgy and Metal Ceramics*, **3–4**: 130 (2017); doi:10.1007/s11106-017-9880-x
12. Z. Zheng, N. Murakamia, J. Liv, Z. Teng, Q. Zhang, Yu Cao, H. Cheng, and T. Ohno, *ChemCatChem.*, **12**: 3783 (2020); https://doi.org/10.1002/cctc.202000366
13. M. V. Shapovalova, T. A. Khalyavka, N. D. Shcherban, O. Y. Khuzhun, V. V. Permyakov, and S. N. Shcherbakov, *Nanosistemi, Nanomateriali, Nanotehnologii*, **18**, Iss. 3: 681 (2020); https://doi.org/10.15407/nnn.18.03.681
14. T. A. Khalyavka, N. D. Shcherban, V. V. Shymanovska, E. V. Manuilov, V. V. Permyakov, and S. N. Shcherbakov, *Res. on Chem. Intermed.*, **45**: 4029 (2019); doi:10.1007/s11164-019-03888-z
15. H. Moradi, A. Eshaghi, S. R. Hosseini, and K. Ghani, *Ultrason. Sonochem.*, **32**: 314 (2016); doi:10.1016/j.ultsonch.2016.03.025
16. Z. Xiong, J. Ma, W. J. Ng, T. D. Waite, and X. S. Zhao, *Water Research*, **45**: 2095 (2011); doi:10.1016/j.watres.2010.12.019
17. J. Ma, Z. Xiong, T. David Waite, W. J. Ng, and X. S. Zhao, *Micropor. Mesopor. Mater.*, **144**: 97 (2011); doi:10.1016/j.micromeso.2011.03.040
18. H. N. Thi-Tuyet, T. A. Thi-Kim, S. N. Van, and N. The-Vinh, *AIMS Mater. Sci.*, **3**: 339 (2016); doi:10.3934/matersci.2016.2.339
19. K. Satyavani S. Gurudeeban, T. Ramanathan, and T. Balasubramanian, *Avicenna J. Med. Biotechnol.*, **4**: 35 (2012).
20. D. Komaraiah, E. Radha, J. Sivakumar, M.V. Ramana Reddy, and R. Sayanna, *Optical Materials*, **108**: 110401 (2020); https://doi.org/10.1016/j.optmat.2020.110401
21. D. Gogo, A. Namdeo, A. K. Golder, and N. R. Peela, *Int. J. Hydrogen Ener-*

gy, **45**: 2729 (2020); https://doi.org/10.1016/j.ijhydene.2019.11.127
22. C. H. Li, Y. H. Hsieh, W. T. Chiu, C. C. Liu, and C. L. Kao, *Separ. Purif. Technol.*, **58**: 148 (2007); doi:10.1016/j.seppur.2007.07.013
23. J. Wang, H. Zhao, X. Liu, X.Li, P. Xu, and X Han, *Catal. Comm.*, **10**: 1052 (2009); https://doi.org/10.1016/j.catcom.2008.12.060
24. L. Der-Shing and Y. W. Chen, *Journal of the Taiwan Institute of Chemical Engineers*, **45**: 705 (2014); https://doi.org/10.1016/j.jtice.2013.07.007
25. W. F. Zhang, Y. L. He, M. S. Zhang, Z. Yin, and Q. Chen, *J. Phys. D: Appl. Phys.*, **33**: 912 (2000); https://iopscience.iop.org/article/10.1088/0022-3727/33/8/305/pdf
26. S. Sahoo, A. K. Arora, and V. Sridharan, *J. Phys. Chem. C*, **113**: 16927 (2009); https://doi.org/10.1021/jp9046193
27. Yu. M. Shul'ga, D. V. Matyushenko, E. N. Kabachkov, A. M. Kolesnikova, E. N. Kurkin, I. A. Domashnev, and S. B. Brichkin, *ZhTF*, **80**: 142 (2010) (in Russian); Ю. М. Шульга, Д. В. Матюшенко, Е. Н. Кабачков, А. М. Колесникова, Е. Н. Куркин, И. А. Домашнев, С. Б. Бричкин, *ЖТФ*, **80**: 142 (2010).
28. A. Ahmad, J. Thiel, and S. Ismat, *J. Phys.: Conf. Ser.*, **61**: 11 (2007); https://iopscience.iop.org/article/10.1088/1742-6596/61/1/003
29. Sajid I. Mogal, Vimal G. Gandhi, Manish Mishra, Shilpa Tripathi, T. Shripathi, Pradyuman A. Joshi, and Dinesh O. Shah, *Ind. Eng. Chem. Res.*, **53**: 5749 (2014); https://doi.org/10.1021/ie404230q
30. S. M. Mali, C. A. Betty, P. N. Bhosale, and P. S. Patil, *Cryst. Eng. Comm.*, **13**: 6349 (2011); doi:10.1039/C1CE05928A
31. W. F. Zhang, M. S. Zhang, Z. Yin, and Q. Chen, *Appl. Phys. B*, **70**: 261 (2000); https://doi.org/10.1007/s003400050043
32. T. O. Busko, O. P. Dmitrenko, M. P. Kulish, M. A. Zabolotnyi, O. O. Prikhod'ko, N. V. Vityuk, A. M. Yeremenko, N. P. Smirnova, A. C. Nikolenko, V. V. Strel'chuk, B. M. Romanyuk, B. V. Shlapats'ka, *Voprosy Atomnoi Nauki i Tekhniki. Seriya: Fizika Radiatsionnykh Povrezhdeniy i Radiatsionnoye Materialovedenie*, **4**: 3 (2011) (in Ukrainian); Т. О. Буско, О. П. Дмитренко, М. П. Куліш, М. А. Заболотний, О. О. Приходько, Н. В. Вітюк, А. М. Єременко, Н. П. Смірнова, А. С. Ніколенко, В. В. Стрельчук, Б. М. Романюк, В. В. Шлапацька, *Вопросы атомной науки и техники. Серия: Физика радиационных повреждений и радиационное материаловедение*, **4**: 3 (2011); http://dspace.nbuv.gov.ua/handle/123456789/111345
33. S. N. Lapach, A. V. Gubenko, and P. N. Babich, *Statistical Methods in Biomedical Research Using Excel* (Kiev: Morion: 2001).